Research Article Vol. 33, No. 1 / 13 Jan 2025 / Optics Express 1329

Optics EXPRESS

Building epsilon near zero materials from layered uniaxial metamaterials

STEPHEN K. GRAY,[1] YOUNGJOON HONG,[2] AND DAVID P. NICHOLLS[3,*]

[1]Center for Nanoscale Materials, Argonne National Laboratory, Lemont, Illinois 60439, USA
[2]Department of Mathematical Sciences, KAIST, 291 Daehak-ro Yuseong-gu, Daejeon 34141, Republic of Korea
[3]Department of Mathematics, Statistics, and Computer Science, University of Illinois at Chicago, 851 South Morgan Street, Chicago, Illinois 60607, USA
[*]davidn@uic.edu

Abstract: Recently, there has been an explosion of activity in the fields of optics and photonics with the advent of fabrication techniques which enable the design of metamaterials which possess properties not encountered in the natural world. In this work, we are concerned with zero permittivity materials and a new scheme to design metamaterials for which all components of the dielectric tensor are approximately zero. Our approach involves the alternate layering of many, very thin, slices of two constituent metamaterials, a uniaxial layered medium and a uniaxial nanowire array. With a simple optimization strategy we demonstrate a candidate configuration which very nearly satisfies our design goal of zero permittivity.

© 2025 Optica Publishing Group under the terms of the Optica Open Access Publishing Agreement

1. Introduction

There has been an explosion of activity over the past twenty years in the fields of optics and photonics with the advent of highly sophisticated fabrication techniques. These have enabled the design and production of materials which are precisely structured on the subwavelength scale of Angströms resulting in "metamaterials" which possess properties not encountered in the natural world. Noteworthy among these are negative index materials [1,2], hyperbolic materials [3–5], and zero index materials [6–13]. (Assuming zero index materials can be achieved, there is also interest in the properties of composite materials containing them [14–16].) Zero index materials are the object of our current study, in particular a *novel* and *explicit* methodology for their realization in metamaterials not only at frequencies away from the plasma frequencies of their constituitive components, but also minimizing dissipative losses.

While our current contribution focuses on materials which have very small permittivities, i.e., the so–called "Epsilon Near Zero" (ENZ) materials, our methodology could readily be adapted to small permeabilities (the "Mu Near Zero" or MNZ materials) or even both (the "Epsilon and Mu Near Zero" or EMNZ materials). The importance of all three of these is difficult to overstate as illustrated in the recent reviews [12,13]. Interesting experimental applications of ENZ materials include antenna design [17], broadband absorbers [18], geometry–independent tunneling [19], and enhancement of nonlinear optical properties [11]. Additionally, it is known (and indeed we will make use of this property) that isotropic ENZ materials are highly reflective and that EMNZ can transmit at all angles of incidence which is desirable for some applications. Particularly promising EMNZ materials are all–dielectric photonic crystals exhibiting certain types of Dirac cones in their photonic band structure [20–22], though it should be noted that these materials can be very challenging to fabricate [21]. Another class of interesting materials are the heavily doped semiconductors discussed in, e.g., [23]. With appropriate doping levels these materials can be designed to have *some* components of their effective permittivity tensor be nearly zero, particularly in the terahertz and mid–infrared spectral ranges. They are very appealing due to

#543178 https://doi.org/10.1364/OE.543178
Journal © 2025 Received 26 Sep 2024; revised 19 Nov 2024; accepted 12 Dec 2024; published 10 Jan 2025

Optics EXPRESS

their compatibility with microelectronic technologies so that they can be incorporated in low–cost, mass–produced structures [23].

Another class of metamaterials garnering significant attention for these purposes are the hyperbolic metamaterials (HMMs) [3–5]. These HMMs are highly anisotropic structures which have a hyperbolic dispersion relation due to the fact that one principal component of the relative permittivity or permeability tensor has the opposite sign of the other two. (In this contribution we focus on non–magnetic materials where the permeability tensor is the identity.) More specifically, if the permittivity tensor is

$$\underline{\underline{\epsilon}} = \begin{pmatrix} \epsilon_x & 0 & 0 \\ 0 & \epsilon_y & 0 \\ 0 & 0 & \epsilon_z \end{pmatrix}, \tag{1}$$

it is not difficult to construct uniaxial ($\epsilon_x = \epsilon_y$) HMMs where $\mathrm{Re}\{\epsilon_x\}\mathrm{Re}\{\epsilon_z\}<0$ [24]. In fact, as outlined in [3–5] there are multiple structures which can realize this goal. The two most prominent are repeated layers of thin films (see Fig. 1(a)) resulting in a uniaxial layered medium (ULM), and periodically placed thin rods in a host structure (see Fig. 1(b)) giving a uniaxial nanowire array (UNA). As detailed in the surveys [3–5] not only are such materials studied for their high anisotropy, but also for the possibility that the components of $\underline{\underline{\epsilon}}$ could be made quite small, i.e., to exhibit ENZ behavior. As we discuss below, while important and interesting, individually these uniaxial metamaterials cannot achieve an effective dielectric constant that has the ENZ property in all three of its diagonal components. In our work we will consider composite systems of ULMs and UNAs, which should provide additional degrees of freedom to achieve ENZ behavior.

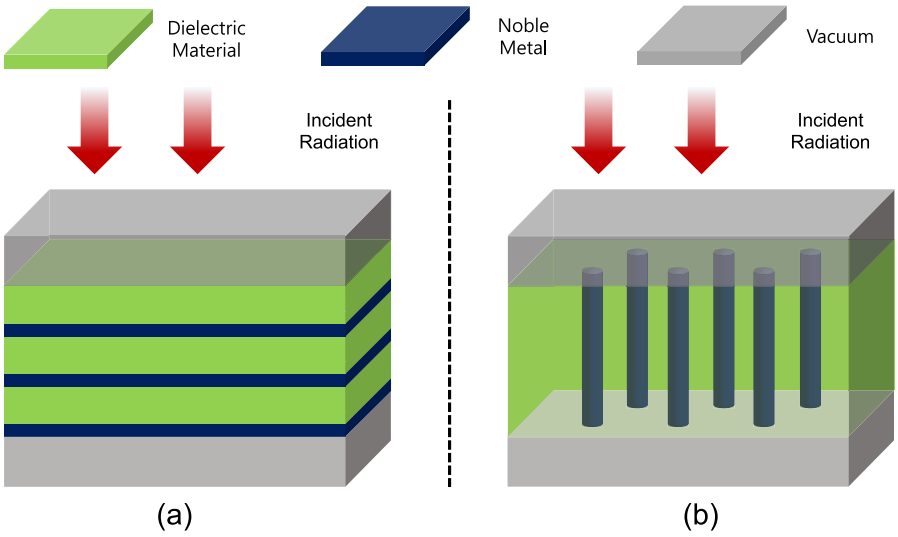

Fig. 1. (a). Depiction of a multiply layered medium which is effectively modeled by a uniaxial layered medium (ULM). (b). Depiction of an array of nanowires in a host medium which is effectively modeled by a uniaxial nanowire array (UNA).

Section 2 below outlines the Effective Medium Theories (EMTs) we utilize and our design goals, including presenting the *novel* EMT we have developed for composite uniaxial materials. Section 3 presents our results, including both EMT and multi–layer Fresnel calculations [25] and Section 4 lists conclusions. The Appendices are devoted to a detailed derivation of our EMT and details of the Fresnel calculations.

Optics EXPRESS

2. Effective medium theories and design goals

In this section we review two existing effective medium theories (EMTs) for uniaxial metamaterials, present our own EMT for mixed uniaxial metamaterials, and state our design goals that the latter permits. Regarding our approach to designing ENZ materials, we point out both the related, but quite different, approach of Sun and Yu (which utilizes Milton's representation) [26], and well–known results upon which we build our current strategy. In particular, it was shown by Rytov [27] (see the Appendix of Wood, Pendry, and Tsai [24] and Appendix 1 of Shekhar, Atkinson, and Jacob [4]) that, in the appropriate scaling regime, if many layers of *isotropic* materials with alternating permittivities $\epsilon^{(1)}$ and $\epsilon^{(2)}$ along the z–axis are constructed in fill fractions $0 \leq p \leq 1$ and $(1-p)$ (see Fig. 1(a)), then the resulting structure is effectively *uniaxial* with components

$$\epsilon_x^{\mathrm{ULM}}\left(p;\epsilon^{(1)},\epsilon^{(2)}\right) := p\epsilon^{(1)} + (1-p)\epsilon^{(2)}, \quad \epsilon_z^{\mathrm{ULM}}\left(p;\epsilon^{(1)},\epsilon^{(2)}\right) := \frac{\epsilon^{(1)}\epsilon^{(2)}}{p\epsilon^{(2)} + (1-p)\epsilon^{(1)}}, \tag{2}$$

$\epsilon_y^{\mathrm{ULM}} = \epsilon_x^{\mathrm{ULM}}$. If the materials are a metal ($\mathrm{Re}(\epsilon^{(1)})<0$) and a dielectric ($\epsilon^{(2)}>0$) then it is easy to see how the real part of $\epsilon_x^{\mathrm{ULM}}$ can be made zero. However, this requires (for $\epsilon^{(1)} \neq \epsilon^{(2)}$)

$$p = \mathrm{Re}\left\{\frac{\epsilon^{(2)}}{\epsilon^{(2)} - \epsilon^{(1)}}\right\}, \quad \epsilon_z^{\mathrm{ULM}} = \frac{\epsilon^{(1)}\epsilon^{(2)}}{\epsilon^{(1)} + \epsilon^{(2)}} \neq 0, \tag{3}$$

so that a true ENZ material cannot be realized since neither $\mathrm{Im}\{\epsilon_x^{\mathrm{ULM}}\}$ nor $\epsilon_z^{\mathrm{ULM}}$ need be small.

In a similar fashion, an array of nanowires can also be configured to deliver an effectively uniaxial material (a uniaxial nanowire array (UNA)). It has permittivity tensor components (see Appendix 2 of Shekhar, Atkinson, and Jacob [4]),

$$\epsilon_x^{\mathrm{UNA}}\left(q;\epsilon^{(3)},\epsilon^{(4)}\right) := \epsilon^{(4)}\left(\frac{(1+q)\epsilon^{(3)} + (1-q)\epsilon^{(4)}}{(1-q)\epsilon^{(3)} + (1+q)\epsilon^{(4)}}\right), \quad \epsilon_z^{\mathrm{UNA}}\left(q;\epsilon^{(3)},\epsilon^{(4)}\right) := q\epsilon^{(3)} + (1-q)\epsilon^{(4)}, \tag{4}$$

$\epsilon_y^{\mathrm{UNA}} = \epsilon_x^{\mathrm{UNA}}$, where the constituent permittivities are $\epsilon^{(3)}$ and $\epsilon^{(4)}$, and the fill fractions are $0 \leq q \leq 1$ and $(1-q)$ (see Fig. 1(b)). We also refer the interested reader to the derivation of a related effective medium theory for nanorods embedded in a gyrotropic material [28]. Again, if the materials are a metal ($\mathrm{Re}(\epsilon^{(3)})<0$) and a dielectric ($\epsilon^{(4)}>0$) then it is easy to see how the real part of $\epsilon_z^{\mathrm{UNA}}$ can be made zero. However, this demands (for $\epsilon^{(3)} \neq \epsilon^{(4)}$ and $\epsilon^{(4)} \neq 0$)

$$q = \mathrm{Re}\left\{\frac{\epsilon^{(4)}}{\epsilon^{(4)} - \epsilon^{(3)}}\right\}, \quad \epsilon_x^{\mathrm{UNA}} = \frac{\epsilon^{(3)}}{2\epsilon^{(4)} + \epsilon^{(3)}} \neq 0, \tag{5}$$

so, again, this is not truly ENZ since neither $\mathrm{Im}\{\epsilon_z^{\mathrm{UNA}}\}$ nor $\epsilon_x^{\mathrm{UNA}}$ need be near zero.

The focus of this paper is to investigate the possibility of layering these two types of metamaterials, a ULM (in fill fraction $0 \leq r \leq 1$) and a UNA (with fill fraction $(1-r)$), into another ULM metamaterial in the hopes of producing one with uniaxial character and *all* components of the permittivity tensor nearly zero

$$\bar{\epsilon}_x = \bar{\epsilon}_y \approx \bar{\epsilon}_z \approx 0. \tag{6}$$

We note that this completely novel approach to designing ENZ improves upon all previous approaches that we have mentioned in that we seek structures which have effective permittivities which satisfy four distinct goals:

1. $\mathrm{Re}\{\bar{\epsilon}_x\} = \mathrm{Re}\{\bar{\epsilon}_y\} \approx 0$,
2. $\mathrm{Im}\{\bar{\epsilon}_x\} = \mathrm{Im}\{\bar{\epsilon}_y\} \approx 0$,

Optics EXPRESS

3. $\mathrm{Re}\{\bar{\epsilon}_z\} \approx 0$, and
4. $\mathrm{Im}\{\bar{\epsilon}_z\} \approx 0$.

If this program can be completed then this amounts to an appropriate choice of the triple (p, q, r). The reason that we pursue the particular layered ULM/UNA structure discussed here is that, with a simple and easy–to–construct structure, we have these *three* (versus *one* for, e.g., a ULM or UNA) independent variables to use for optimization. However, further guidance is required in the form of an effective medium theory for *uniaxial* materials which appears to be missing from the literature. A central contribution of this work is to provide this theory (see Appendix A for details) for layered *uniaxial* media resulting in the novel formulas

$$\begin{aligned} \bar{\epsilon}_x\left(p, q, r; \epsilon_x^{\mathrm{ULM}}, \epsilon_x^{\mathrm{UNA}}\right) &:= r\epsilon_x^{\mathrm{ULM}} + (1-r)\epsilon_x^{\mathrm{UNA}}, \\ \bar{\epsilon}_z\left(p, q, r; \epsilon_z^{\mathrm{ULM}}, \epsilon_z^{\mathrm{UNA}}\right) &:= \frac{\epsilon_z^{\mathrm{ULM}}\epsilon_z^{\mathrm{UNA}}}{r\epsilon_z^{\mathrm{UNA}} + (1-r)\epsilon_z^{\mathrm{ULM}}}, \end{aligned} \tag{7}$$

for $\bar{\epsilon}_y = \bar{\epsilon}_x$, c.f. (39). Our other addition is to show how a rather simple optimization scheme can be used to deliver structures with quite small values of *both* $\bar{\epsilon}_x$ and $\bar{\epsilon}_z$ simultaneously, equivalent to the four goals listed above, which we believe are viable candidates for true ENZ materials. It should be noted that in the ENZ regime nonlinear effects will play an enhanced role [29,30]. One could contemplate additional terms in our formula above to account for this, however, as we currently use this simply for *prediction*, we leave these concerns for future work.

3. Design of ENZ metamaterials from layered ULM/UNA

From our discussion above, it is clear that one simple approach to find a candidate ENZ material is to discover a triple (p, q, r) such that we minimize the quantity

$$f(p, q, r; \epsilon_x^{\mathrm{ULM}}, \epsilon_z^{\mathrm{ULM}}, \epsilon_x^{\mathrm{UNA}}, \epsilon_z^{\mathrm{UNA}}) := \left|\bar{\epsilon}_x\left(p, q, r; \epsilon_x^{\mathrm{ULM}}, \epsilon_x^{\mathrm{UNA}}\right)\right|^2 + \left|\bar{\epsilon}_z\left(p, q, r; \epsilon_z^{\mathrm{ULM}}, \epsilon_z^{\mathrm{UNA}}\right)\right|^2. \tag{8}$$

There are many approaches to finding a minimal value $f_{\min}$ at $(p_{\min}, q_{\min}, r_{\min})$, if it exists [31], however, as the function is quite simple, we opted for a "brute force" approach where we discretized the cube $[0, 1] \times [0, 1] \times [0, 1]$ in (p, q, r) with (N_p, N_q, N_r) equally spaced points and found the minimal value of f on this grid. We note that this delivers the optimal solution up to precision $(1/N_p, 1/N_q, 1/N_r)$ in (p, q, r) space.

It should be noted that even achieving p, q, r such that f is quite small only indicates conditions (relative material amounts) such that isotropic ENZ behavior might be achieved because the underlying effective mediums are approximations. Finite–sized and multi–layered candidate structures consistent with p, q, r need to be devised and tested with more rigorous electrodynamics simulations.

3.1. Candidate ENZ metamaterials

To demonstrate the capabilities of our scheme for delivering an ENZ metamaterial we decided to simplify our design parameters and search among the class of structures with one complex (specifically metallic) and one positive real dielectric constant (i.e., $\epsilon^{(1)} = \epsilon^{(3)} \in \mathbf{C}$ and $\epsilon^{(2)} = \epsilon^{(4)} \in \mathbf{R}$) and we now suppress any reference to $\epsilon^{(3)}$ and $\epsilon^{(4)}$. We also fixed the value of the dielectric to be a constant value representative of those found among materials common in such structures. More specifically, we chose $\epsilon^{(2)} = 2.25$ which is representative for silica. It is well known that the noble metals (e.g., silver) have permittivities which are strongly dependent

Optics EXPRESS

upon illumination frequency. To accommodate this state of affairs, rather than select a *single* value of $\epsilon^{(1)}$, we chose to sweep over a wide range of possible values

$$-20 \leq \mathrm{Re}\{\epsilon^{(1)}\} \leq 0, \quad 0 \leq \mathrm{Im}\{\epsilon^{(1)}\} \leq 5, \tag{9}$$

and identified a triple $(p_{\min}, q_{\min}, r_{\min})$ which minimizes $f(p,q,r)$ at each. Finally, we settled upon a discretization of the unit cube in (p,q,r) space with $N_p = N_q = N_r = 101$ points, and an approximation of the space of $\epsilon^{(1)}$ by $N_{\mathrm{re}} = N_{\mathrm{im}} = 401$ equally–spaced grid points.

In Fig. 2 we display a plot of $f_{\min}$ in the case $\epsilon^{(2)} = 2.25$, and the corresponding values of $p_{\min}$ (Fig. 3), $q_{\min}$ (Fig. 4), and $r_{\min}$ (Fig. 5). Here we see a broad range of values of $\epsilon^{(1)}$ for which $f_{\min}$ is quite small (on the order of 10^{-2}). More specifically, this region is certainly contained in the rhombus specified by the region on the plot to the left of the line from $\epsilon^{(1)} = -5$ to $\epsilon^{(1)} = -20 + 2i$. This certainly contains the values of $\epsilon^{(1)}$ for silver over a wide range of illumination frequencies. However, we do point out that many of these values are *not* realized by silver or any other metal. For this reason, in the next section we investigate structures which *do* correspond to values achieved by silver at certain illumination frequencies.

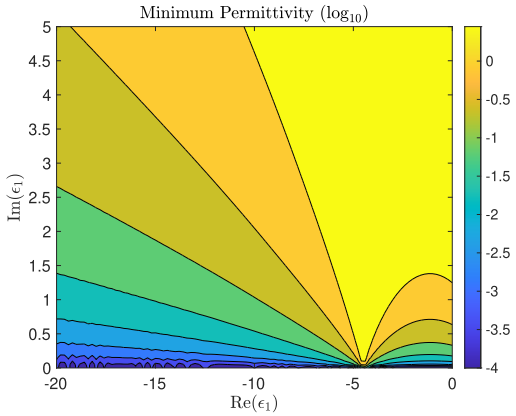

Fig. 2. Results for a fixed dielectric with permittivity value $\epsilon^{(2)} = 2.25$: Plot of the minimum value of the logarithm of the modulus of the effective permittivity, $(\bar{\epsilon}_x, \bar{\epsilon}_z)$, of the metamaterial, $\log_{10}(f(p,q,r))$, as a function of $\epsilon^{(1)}$.

3.2. ENZ behavior

While the formulas (7) allow one to identify ENZ behavior in a specific and quantitative fashion, this is only an effective theory and we would like to verify that a particular structure displays true ENZ behavior. The seminal paper [8] identified several properties of ENZ materials including one that we will identify as "diagnostic." Consider an infinitely extended ENZ slab of thickness t, illuminated by a transverse magnetic (TM) planewave at reference plane $\{z = d\}$ with angle of incidence θ. With a rather explicit computation [8] showed that the reflection and transmission coefficients in this configuration are

$$\lim_{\epsilon\to 0} R(\epsilon,\theta) = \begin{cases} -\frac{k_0 t e^{ik_0 d}}{2i + k_0 t}, & \theta = 0, \\ -e^{-ik_0 d}, & \theta \neq 0, \end{cases} \quad \lim_{\epsilon\to 0} T(\epsilon,\theta) = \begin{cases} -\frac{e^{ik_0 d}}{1 - i(k_0 t)/2}, & \theta = 0, \\ 0, & \theta \neq 0. \end{cases} \tag{10}$$

In other words, *no* transmission occurs through an ENZ material unless the incidence direction is identically orthogonal to the flat interface. Therefore, we treat as a diagnostic of ENZ behavior, a "Transmission Map" (a plot of transmission versus incidence angle) that is identically zero save

Optics EXPRESS

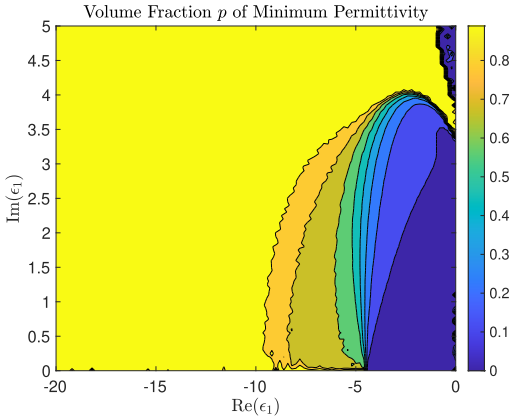

Fig. 3. Results for a fixed dielectric with permittivity value $\epsilon^{(2)} = 2.25$: Plot of the value of p at the minimum, $p_{\min}$, as a function of $\epsilon^{(1)}$.

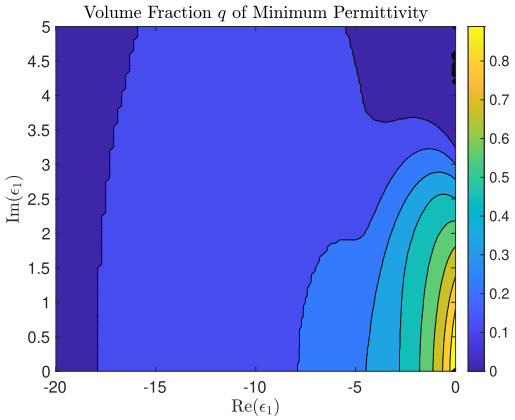

Fig. 4. Results for a fixed dielectric with permittivity value $\epsilon^{(2)} = 2.25$: Plot of the value of q at the minimum, $q_{\min}$, as a function of $\epsilon^{(1)}$.

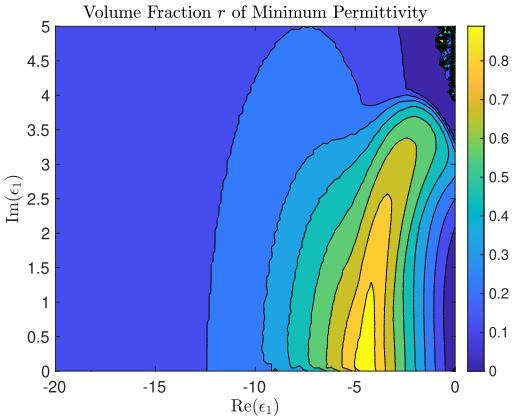

Fig. 5. Results for a fixed dielectric with permittivity value $\epsilon^{(2)} = 2.25$: Plot of the value of r at the minimum, $r_{\min}$, as a function of $\epsilon^{(1)}$.

Optics EXPRESS

at $\theta = 0$ which has a finite spike. We point out that this particular transmission behavior, as noted in [8], represents an angular filter which is relevant in some applications. Some experimentally realized ENZ materials, based only on a ULM (see, e.g., [9–11]) alone, *cannot* act as such filters as they permit non–negligible transmission at *all* angles of incidence. We chose selective transmission as a measure of likely isotropic ENZ behavior in practice. Other measures, e.g. phase changes, could also be devised. For actual finite–sized, multi–layered materials "true" isotropic ENZ behavior may be difficult to completely validate but at least performance consistent with ENZ materials might be achieved.

To identify a realistic structure amenable to our approach we considered a silver/silica combination for which we chose, as before, $\epsilon^{(2)} = 2.25$ and $\epsilon^{(1)}$ from the values reported in Johnson and Christy [32] for silver over a range of illumination wavelengths $187.9\,\text{nm} \le \lambda_j \le 1937.0\,\text{nm}$. Note that silver/silica ENZ materials have been experimentally realized, e.g., Refs. [9] and [11].

We had in mind a device of total thickness $t^{\text{total}} = 1200$ nm with $M = 10$ layer pairs (each pair of thickness $t^{\text{pair}} = 120$ nm) so we restricted the range $0.2 \le r \le 0.8$ resulting in layers that were at least 24 nm thick, since thinner layers may be both difficult to fabricate and less homogeneous. We further restricted $0.2 \le p, q \le 0.8$ so that these layers are also not unreasonably thin, and minimized f for each λ_j. The minimal value of f, $f_{\text{min}} = 0.0356373$, occurred at $\lambda = 471.4$ nm (where $\epsilon_{\text{Ag}} = -8.22866 + 0.2869i$), with

$$p_{\text{min}} = 0.687654, \quad q_{\text{min}} = 0.214277, \quad r_{\text{min}} = 0.499289. \tag{11}$$

To examine the practicality of producing such a structure we approximate $p_{\text{min}} \approx p_{\text{approx}} = 0.688$, $q_{\text{min}} \approx q_{\text{approx}} = 0.214$, and $r_{\text{min}} \approx r_{\text{approx}} = 0.499$, which delivers effective medium layers with thicknesses

$$t^{\text{ULM}} = r_{\text{min}} \times 120\,\text{nm} \approx 59.88\,\text{nm}, \quad t^{\text{UNA}} = (1 - r_{\text{min}}) \times 120\,\text{nm} \approx 60.12\,\text{nm}. \tag{12}$$

(We have verified that the abrupt truncation of significant figures in p, q and r, carried out for convenience of material design, does not significantly affect the transmission properties.) Within each ULM layer we have fill fractions

$$t^{\text{ULM,Ag}} = p_{\text{min}} \times r_{\text{min}} \times 120\,\text{nm} \approx 41.1974\,\text{nm}, \quad t^{\text{ULM,SiO}_2} = (1 - p_{\text{min}}) \times r_{\text{min}} \times 120\,\text{nm} \approx 18.6826\,\text{nm}, \tag{13}$$

so that if the ULM layers consist of, say, four layer pairs then each is roughly 12 – 4.5 nm. For a UNA layer, q gives the ratio of areas of the nanowires in a unit cell to the area of the unit cell, $q = a/A = L(\pi d^2/4)/A$, where L is the number of nanowires (of diameter d) in the unit cell. Shekhar, Atkinson, and Jacob [4] list $L = 3$ for a hexagonal lattice and so, with this, $d = \sqrt{4Aq/(3\pi)}$. If we select $A = 50 \times 50\,\text{nm}^2$ and $q_{\text{min}} = 0.2$ we realize a rod diameter of $d = 15$ nm.

Having identified these values we considered a structure with $M = 10$ flat ULM/UNA layer pairs with compositions specified by $(p_{\text{min}}, q_{\text{min}}, r_{\text{min}})$ given above (Fig. 6 shows a schematic for $M = 5$). With a simple Fresnel solver (see Appendix B) we simulated the planewave scattering of TM waves by this structure at angle of incidence θ from the normal to compute the Transmission Map defined above. We conducted this diagnostic and in Fig. 7 we display the Transmission Map. This figure features three curves:

- In blue ("Multilayer"), the output of our Fresnel solver with $M = 10$ layers of ULM (with permittivity components $(\epsilon_x^{\text{ULM}}, \epsilon_z^{\text{ULM}})$) and $M = 10$ layers of UNA (with permittivity components $(\epsilon_x^{\text{UNA}}, \epsilon_z^{\text{UNA}})$).
- In green ("EMT"), the output of our Fresnel solver with one layer of effective material (with permittivity components $(\bar{\epsilon}_x, \bar{\epsilon}_z)$).

Optics EXPRESS

- In red ("ENZ"), the output of our Fresnel solver with one layer of (approximate) "true" ENZ with $\epsilon = \epsilon_x = \epsilon_z = 10^{-6}$.

Here the red curve is our "goal" while the green curve was our guide and the blue curve is what we can actually realize. While the blue/green curves do not overlay the red one due to dissipation (strictly positive imaginary part of the permittivity of silver), the shape and characteristics are quite similar and we view this as a viable candidate for an ENZ. The final test of the feasibility of our approach would be a "full wave" simulation where each of the effective ULM and effective UNA layers would be replaced with actual metal/dielectric structures. While such a construction for the UNA layers is beyond the scope of our current numerical implementation, we replaced each of the effective ULM layers with $N = 4$ silver/silica layer pairs and conducted the same numerical experiment outlined above. The results are depicted in Fig. 8 where the "Multilayer" and "EMT" curves are the same, and our new simulation is labelled "FW" (cyan). We note that, while this new curve is somewhat less peaked than our "Multilayer" simulation due to its effective nature, we are encouraged by the nearly ENZ behavior which this more realistic structure exhibits.

To further illustrate the capabilities of our approach we reconsidered the calculation above with silver replaced by gold. Thus, we considered a gold/silica structure for which $\epsilon^{(2)} = 2.25$ and $\epsilon^{(1)}$ was chosen from the values reported in Johnson and Christy [32] for gold over a range of illumination wavelengths $187.9\,\text{nm} \leq \lambda_j \leq 1937.0\,\text{nm}$. As before, the device was of total thickness $t^{\text{total}} = 1200$ nm with $M = 10$ layer pairs (each pair of thickness $t^{\text{pair}} = 120$ nm). Once again, we restricted the ranges $0.2 \leq p, q, r \leq 0.8$ and minimized f for each λ_j. The minimal value of f, $f_{\text{min}} = 0.655371$, occurred at $\lambda = 616.8$ nm (where $\epsilon_{\text{Au}} = -10.6619 + 1.37424i$), with

$$p_{\text{min}} = 0.799034, \quad q_{\text{min}} = 0.2, \quad r_{\text{min}} = 0.335083. \tag{14}$$

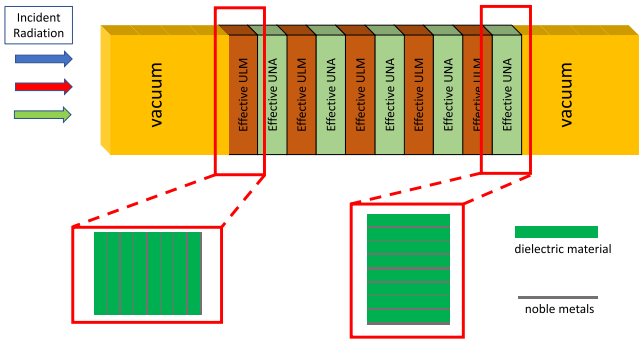

Fig. 6. Depiction of multiply layered medium composed of ULM and UNA bilayers.

Again, having identified these values we considered a structure with $M = 10$ flat ULM/UNA layer pairs with compositions specified by $(p_{\text{min}}, q_{\text{min}}, r_{\text{min}})$ given above (see Fig. 6). With our Fresnel solver (see Appendix B) we simulated the planewave scattering of TM waves by this structure at angle of incidence θ from the normal to compute the Transmission Map. We conducted this diagnostic and in Fig. 9 we display our results with the "Multilayer," "EMT," and "ENZ" curves. Once again, while the blue/green curves do not overlay the red one due to dissipation, the shape and characteristics are quite similar and we view this as another candidate for an ENZ.

Once again, we also conducted our (approximate) "full wave" simulation where each of the effective ULM layers was replaced with $N = 4$ gold/silica layer pairs. The results are shown in Fig. 10 where the "Multilayer" and "EMT" curves are the same, and our new simulation is labelled "FW" (cyan). In this case the new curve is less peaked but taller than our "Multilayer"

Optics EXPRESS

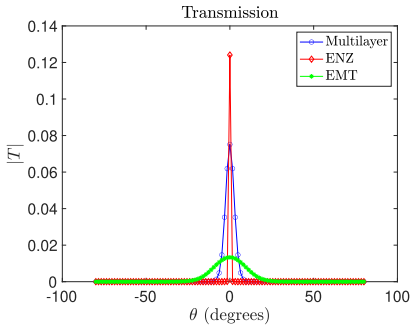

Fig. 7. Plot of the Transmission Map as a function of angle of incidence, θ, at $\lambda = 471.4$ nm for the silver/silica ($\epsilon^{(2)} = 2.25$) multilayered structure we have constructed (blue), the bulk metamaterial configuration (green), and an idealized ENZ material (red; $\epsilon = 10^{-6}$).

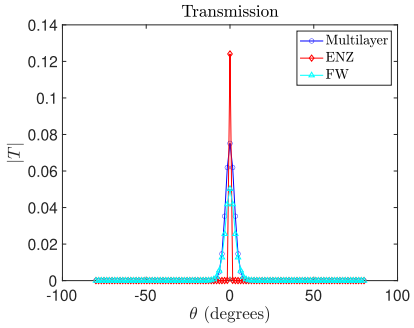

Fig. 8. Plot of the Transmission Map as a function of angle of incidence, θ, at $\lambda = 471.4$ nm for the silver/silica ($\epsilon^{(2)} = 2.25$) multilayered structure we have constructed (blue), the full–wave simulation (cyan), and an idealized ENZ material (red; $\epsilon = 10^{-6}$).

simulation due to its effective nature. However, as before, we note the nearly ENZ behavior which this more realistic structure exhibits. We note that the normal incidence transmission from the full wave result (the cyan "FW" curve) in Fig. 10 is actually above those for an ideal ENZ which is a somewhat surprising and perhaps an accidental finite–size effect.

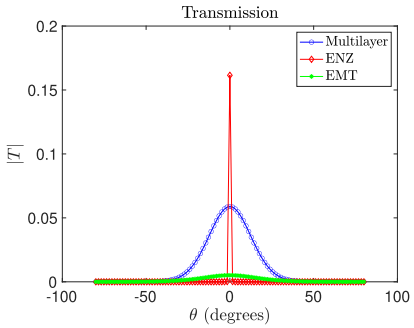

Fig. 9. Plot of the Transmission Map as a function of angle of incidence, θ, at $\lambda = 616.8$ nm for the gold/silica ($\epsilon^{(2)} = 2.25$) multilayered structure we have constructed (blue), the bulk metamaterial configuration (green), and an idealized ENZ material (red; $\epsilon = 10^{-6}$).

Optics EXPRESS

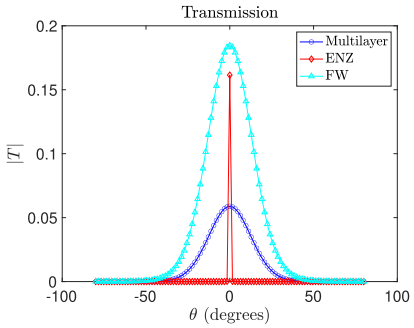

Fig. 10. Plot of the Transmission Map as a function of angle of incidence, θ, at $\lambda = 616.8$ nm for the gold/silica ($\epsilon^{(2)} = 2.25$) multilayered structure we have constructed (blue), the full–wave simulation (cyan), and an idealized ENZ material (red; $\epsilon = 10^{-6}$).

4. Conclusions

In this paper, we have demonstrated a new scheme for building an ENZ material as a multiple layering of two uniaxial metamaterials: a uniaxial layered medium (ULM) and a uniaxial nanowire array (UNA). To guide our strategy we have devised a novel Effective Medium Theory which generalizes the classical result to layered *uniaxial* materials. Through a straightforward minimization scheme we devised candidate silver/silica and gold/silica structures and evaluated their performance in delivering transmission only at normal incidence (a property of true ENZ materials) at a particular operating wavelength. We were able to demonstrate promising results with our new design procedure. However we stress that there is considerable room for improvement in order to suggest practical devices that could be used to efficiently filter light or generate enhanced nonlinear optical responses.

Appendix A: effective medium theory for layered uniaxial materials

In this section, we derive an effective medium theory (EMT) for layers of uniaxial materials. Our presentation is quite similar in spirit to that of Wood, Pendry, and Tsai [24], however, rather than computing the eigenvalues of the transmission operator, we focus on powers of this matrix. We found this strategy to be far less cumbersome while delivering the same result.

A1. Governing equations

We consider a multilayer grating structure composed of flat layers of different uniaxial materials with varying thicknesses. To be more precise, uniaxial materials occupy each of the $(M+1)$–many domains

$$S^0 := \{z > g_1\}; \quad S^M := \{z < g_M\}; \quad S^m := \{g_{m+1} < z < g_m\}, \quad 1 \le m \le M-1; \tag{15}$$

where the (flat) interface locations are given by $\{z = g_m\}_{m=1}^{M}$. This structure is illuminated by incident radiation of frequency ω and angle θ in the uppermost (vacuum) layer, S^0, of the form

$$\underline{v}^{\text{inc}} = e^{-i\omega t + i\alpha x - i\gamma z}, \quad \alpha = k_0 \sin(\theta), \quad \gamma = k_0 \cos(\theta), \quad k_0 = \omega/c_0, \tag{16}$$

Optics EXPRESS

and c_0 is the speed of light in the vacuum. Factoring out time dependence of the form $\exp(-i\omega t)$ we define the (reduced) scattered fields

$$v_m = v_m(x,z), \quad \text{in } S^m \text{ for } 0 \le m \le M, \tag{17}$$

and seek α-quasiperiodic, outgoing (upward/downward propagating) solutions of the following system of Helmholtz equations [25,33]

$$\begin{aligned}
&\operatorname{div}[A_m \nabla v_m] + k_0^2 v_m = 0, && \text{in } S^m, 0 \le m \le M, && \text{(18a)}\\
&v_0 - v_1 = -e^{i\gamma g_1} e^{i\alpha x}, && \text{at } z = g_1, && \text{(18b)}\\
&\tau_0 \partial_z v_0 - \tau_1 \partial_z v_1 = \tau_0 (i\gamma) e^{i\gamma g_1} e^{i\alpha x}, && \text{at } z = g_1, && \text{(18c)}\\
&v_m - v_{m+1} = 0, && \text{at } z = g_m, 1 \le m \le M-1, && \text{(18d)}\\
&\tau_m \partial_z v_m - \tau_{m+1} \partial_z v_{m+1} = 0, && \text{at } z = g_m, 1 \le m \le M-1, && \text{(18e)}
\end{aligned}$$

where

$$A_m = \begin{pmatrix} 1/\epsilon_{m,z} & 0 \\ 0 & 1/\epsilon_{m,x} \end{pmatrix}, \quad \tau_m = \begin{cases} 1, & \text{Transverse Electric (TE)}, \\ 1/\epsilon_{m,x}, & \text{Transverse Magnetic (TM)}, \end{cases} \quad 0 \le m \le M. \tag{19}$$

Rather than solve these Fresnel equations directly (which would yield the scattered fields) we pursue a simplified configuration (with a single layer) whose governing equations are "effectively" the same. More specifically, we study operators which have the effect of transmitting scattered fields (which satisfy the relevant Helmholtz equation) from one layer interface, say $\{z = g_m\}$, to the next one down, in this case $\{z = g_{m+1}\}$. Our goal is to "equate" a sequence of these Transmission Operators (TOs) for the multiply layered structure to the TO of a single layer configuration.

A2. Transmission operators

To derive our EMT we recall the TO of a uniaxial material layer of thickness h, which maps Dirichlet and Neumann data at the upper interface of the layer $\{z = g_m = h\}$ to the same data at the lower interface $\{z = g_{m+1} = 0\}$, is

$$T : \begin{pmatrix} v(x,h) \\ \tau \partial_z v(x,h) \end{pmatrix} \to \begin{pmatrix} v(x,0) \\ \tau \partial_z v(x,0) \end{pmatrix}, \quad \tau = \begin{cases} 1, & \text{Transverse Electric (TE)}, \\ 1/\epsilon_x, & \text{Transverse Magnetic (TM)}, \end{cases} \tag{20}$$

(see [33]). We now seek to equate the action of an M–layer structure of thickness $H = \sum_{m=1}^{M} h_m$ with a single uniaxial layer of the same thickness, H, with *effective* parameters $\{\bar{\epsilon}_x, \bar{\epsilon}_z\}$. To do this we enforce the equality of the TOs

$$\bar{T}(\bar{\epsilon}_x, \bar{\epsilon}_z) \approx \prod_{m=1}^{M} T(m), \tag{21}$$

and send $H \to 0$ (which implies that the h_m tend to zero as well).

Optics EXPRESS

First, in each homogeneous layer of thickness h we can express [33]

$$v(x,z) = \left\{ A\cos(\gamma(z-h)) + \frac{B}{\tau\gamma}\sin(\gamma(z-h)) \right\} e^{i\alpha x}, \tag{22}$$

where

$$\frac{\alpha^2}{\epsilon_z} + \frac{\gamma^2}{\epsilon_x} = k_0^2 \quad \Longrightarrow \quad \gamma^2 = \epsilon_x k_0^2 - \frac{\epsilon_x}{\epsilon_z}\alpha^2, \tag{23}$$

implying that

$$\tau\partial_z v(x,z) = \{-\tau\gamma A\sin(\gamma(z-h)) + B\cos(\gamma(z-h))\}\, e^{i\alpha x}. \tag{24}$$

With these it is easy to see that

$$v(x,h) = Ae^{i\alpha x}, \tag{25a}$$

$$\tau\partial_z v(x,h) = Be^{i\alpha x}, \tag{25b}$$

$$v(x,0) = \left\{ A\cos(\gamma h) - \frac{B}{\tau\gamma}\sin(\gamma h) \right\} e^{i\alpha x}, \tag{25c}$$

$$\tau\partial_z v(x,0) = \{\tau\gamma A\sin(\gamma h) + B\cos(\gamma h)\}\, e^{i\alpha x}, \tag{25d}$$

so that the TO is given by

$$T\left[\begin{pmatrix} A \\ B \end{pmatrix} e^{i\alpha x}\right] = \begin{pmatrix} \cos(\gamma h) & -\sin(\gamma h)/(\tau\gamma) \\ \tau\gamma\sin(\gamma h) & \cos(\gamma h) \end{pmatrix} \begin{pmatrix} A \\ B \end{pmatrix} e^{i\alpha x}. \tag{26}$$

Now, the TO for the M–layer structure is clearly

$$T^M = \prod_{m=1}^{M} T(m). \tag{27}$$

However, we choose not to form this product as it is not only wildly complicated, but also unnecessary. Instead, we keep in mind that we consider H small, so that the h_m are even smaller, and we may approximate

$$T = \begin{pmatrix} \cos(\gamma h) & -\sin(\gamma h)/(\tau\gamma) \\ \tau\gamma\sin(\gamma h) & \cos(\gamma h) \end{pmatrix} = \begin{pmatrix} 1 & 0 \\ 0 & 1 \end{pmatrix} + \begin{pmatrix} 0 & -1/\tau \\ \tau\gamma^2 & 0 \end{pmatrix} h + O(h^2) = I + T_1 h + O(h^2). \tag{28}$$

It is not difficult to see that, due to the leading identity operator,

$$T^M = I + \sum_{m=1}^{M} T_1(m)h_m + O(h_{\max}^2), \quad T_1(m) = \begin{pmatrix} 0 & -1/\tau_m \\ \tau_m\gamma_m^2 & 0 \end{pmatrix}, \quad h_{\max} := \max_{1\le m\le M} h_m. \tag{29}$$

If we now fix upon transverse magnetic polarization (so that $\tau_m = 1/\epsilon_{m,x}$) and use the definitions of γ_m^2, we further discover that

$$T^M = I + \begin{pmatrix} 0 & -\sum_{m=1}^{M} h_m\epsilon_{m,x} \\ Hk_0^2 - \alpha^2\sum_{m=1}^{M} h_m/\epsilon_{m,z} & 0 \end{pmatrix} + O(H^2). \tag{30}$$

Optics EXPRESS

A3. Effective bulk layer

From the developments of the previous section, the TO of the effective bulk layer is clearly

$$\bar{T} = \begin{pmatrix} \cos(\bar{\gamma}H) & -\sin(\bar{\gamma}H)/(\bar{\tau}\bar{\gamma}) \\ \bar{\tau}\bar{\gamma}\sin(\bar{\gamma}H) & \cos(\bar{\gamma}H) \end{pmatrix}, \tag{31}$$

c.f. (26), and, again using the smallness assumption for H and focusing on TM polarization, we discover

$$\bar{T} = I + \begin{pmatrix} 0 & -1/\bar{\tau} \\ \bar{\tau}\bar{\gamma}^2 & 0 \end{pmatrix} H + O(H^2) = I + \begin{pmatrix} 0 & -\bar{\epsilon}_x \\ k_0^2 - \alpha^2/\bar{\epsilon}_z & 0 \end{pmatrix} H + O(H^2). \tag{32}$$

If we now equate (30) and (32) up to order H we find

$$-\sum_{m=1}^{M} h_m \epsilon_{m,x} = -\bar{\epsilon}_x H, \tag{33a}$$

$$Hk_0^2 - \alpha^2 \sum_{m=1}^{M} h_m/\epsilon_{m,z} = k_0^2 H - (\alpha^2/\bar{\epsilon}_z)H, \tag{33b}$$

which gives,

$$H\bar{\epsilon}_x = \sum_{m=1}^{M} h_m \epsilon_{m,x}, \qquad \frac{H}{\bar{\epsilon}_z} = \sum_{m=1}^{M} \frac{h_m}{\epsilon_{m,z}}. \tag{34}$$

We note that in the case of homogeneous materials ($\epsilon_{m,x} = \epsilon_{m,z} = \epsilon_m$) this reduces to

$$H\bar{\epsilon}_x = \sum_{m=1}^{M} h_m \epsilon_m, \qquad \frac{H}{\bar{\epsilon}_z} = \sum_{m=1}^{M} \frac{h_m}{\epsilon_m}, \tag{35}$$

which matches the result of Wood, Pendry, and Tsai [24]. We further point out that if

$$M = 2, \quad h_1 = rH, \quad \epsilon_{1,x} = \epsilon_x^{\mathrm{ULM}}, \quad \epsilon_{1,z} = \epsilon_z^{\mathrm{ULM}}, \quad h_2 = (1-r)H, \quad \epsilon_{2,x} = \epsilon_x^{\mathrm{UNA}}, \quad \epsilon_{2,z} = \epsilon_z^{\mathrm{UNA}}, \tag{36}$$

then (34) gives

$$H\bar{\epsilon}_x = rH\epsilon_x^{\mathrm{ULM}} + (1-r)H\epsilon_x^{\mathrm{UNA}}, \qquad \frac{H}{\bar{\epsilon}_z} = \frac{rH}{\epsilon_x^{\mathrm{ULM}}} + \frac{(1-r)H}{\epsilon_z^{\mathrm{UNA}}}, \tag{37}$$

which, upon cancelling the common factors of H, delivers

$$\bar{\epsilon}_x = r\epsilon_x^{\mathrm{ULM}} + (1-r)\epsilon_x^{\mathrm{UNA}}, \qquad \frac{1}{\bar{\epsilon}_z} = \frac{r}{\epsilon_z^{\mathrm{ULM}}} + \frac{(1-r)}{\epsilon_z^{\mathrm{UNA}}}. \tag{38}$$

Combining the right hand side of the latter equation and taking the reciprocal gives

$$\bar{\epsilon}_x = r\epsilon_x^{\mathrm{ULM}} + (1-r)\epsilon_x^{\mathrm{UNA}}, \qquad \bar{\epsilon}_z = \frac{\epsilon_z^{\mathrm{ULM}}\epsilon_z^{\mathrm{UNA}}}{r\epsilon_z^{\mathrm{UNA}} + (1-r)\epsilon_z^{\mathrm{ULM}}}. \tag{39}$$

Optics EXPRESS

Appendix B: Fresnel solver

To complete the discussion of our numerical simulations, we briefly outline our Fresnel solver which, in infinite precision, delivers the *exact* solution of the uniaxial homogeneous–layer, flat–interface problem. We note that this solver trivially generalizes the classical solution procedure for the *isotropic* homogeneous–layer, flat–interface problem discussed in Chapter 5 of the text of Yeh [25]. Our approach gives a solution to the governing Eqs. (18), beginning with the fact that the α–quasiperiodic solutions of the Helmholtz equations, (18a), are

$$v_m(x,z) = \left\{ D_m e^{-i\gamma_m(z-g_m)} + U_m e^{i\gamma_m(z-g_{m+1})} \right\} e^{i\alpha x}, \quad 0 \le m \le M, \tag{40}$$

where

$$\alpha = \sqrt{\epsilon_0} k_0 \sin(\theta), \quad \gamma_m = \sqrt{\epsilon_{m,x}\left(k_0^2 - \frac{\alpha^2}{\epsilon_{m,z}}\right)}. \tag{41}$$

The upward/downward propagating conditions demand that $D_0 = U_M = 0$, while the interfacial boundary conditions, (18b–18e), give a *linear* system of $(2M)$ equations for the $(2M)$ unknowns, $\{U_1, D_2, U_2, \ldots, D_{M-1}, U_{M-1}, D_M\}$. More specifically, these governing equations are

$$A\vec{V} = \vec{R}, \tag{42}$$

where

$$A = \begin{pmatrix}
1 & -1 & -\Gamma_1 & 0 & \cdots & 0 \\
\tau_{0,z}\gamma_0 & \tau_{1,z}\gamma_1 & -\tau_{1,z}\gamma_1\Gamma_1 & 0 & \cdots & 0 \\
 & & \ddots & \ddots & & \\
\cdots & \Gamma_{m-1} & 1 & -1 & \Gamma_m & \cdots \\
\cdots & -\tau_{m-1,z}\gamma_{m-1}\Gamma_{m-1} & \tau_{m-1,z}\gamma_{m-1} & \tau_m\gamma_m & \tau_m\gamma_m\Gamma_m & \cdots \\
 & & \ddots & \ddots & & \\
0 & \cdots & 0 & \Gamma_{M-1} & 1 & -1 \\
0 & \cdots & 0 & -\tau_{M-1,z}\gamma_{M-1}\Gamma_{M-1} & \tau_{M-1,z}\gamma_{M-1} & \tau_{M,z}\gamma_M
\end{pmatrix}, \tag{43}$$

and

$$\Gamma_m := e^{i\gamma_m h_m}, \quad h_m := g_{m-1} - g_m, \tag{44}$$

and

$$\vec{V} = \begin{pmatrix} U_1 \\ D_2 \\ U_2 \\ \vdots \\ D_{M-1} \\ U_{M-1} \\ D_M \end{pmatrix}, \quad \vec{R} = e^{-i\gamma_0 g_1} \begin{pmatrix} -1 \\ \tau_{0,z}\gamma_0 \\ 0 \\ \vdots \\ 0 \\ 0 \\ 0 \end{pmatrix}. \tag{45}$$

Once the $\vec{V}$ has been recovered the scattered solution can be computed *anywhere* as can useful quantities of interest, such as the reflection and transmission coefficients,

$$R = U_1 e^{-i\gamma_0 g_1}, \quad T = D_M e^{i\gamma_{M+1} g_M}. \tag{46}$$

Optics EXPRESS

Therefore, in considering the scattering returns from a structure with $(M + 1)$–many homogeneous uniaxial layers (uncluding the unbounded upper and lower regions) with permittivities $\{\epsilon_{m,x}, \epsilon_{m,z}\}$, $0 \leq m \leq M$ and interfaces located at $z = g_m$, $1 \leq m \leq M$, we simply solve (42) using Gaussian elimination and produce, e.g., the reflection and transmission coefficients from the formulas (46).

Funding. Directorate for Mathematical and Physical Sciences (DMS-2111283); National Research Foundation of Korea (NRF-2021R1A2C1093579, RS-2023-00219980); U.S. Department of Energy (DE-AC02-06CH11357).

Acknowledgment. Work performed at the Center for Nanoscale Materials, a U.S. Department of Energy Office of Science User Facility, was supported by the U.S. DOE, Office of Basic Energy Sciences, under Contract No. DE-AC02-06CH11357.

Disclosures. The authors declare no conflicts of interest.

Data availability. Data underlying the results presented in this paper are not publicly available at this time but may be obtained from the authors upon reasonable request.

References

1. V. Veselago, "The electrodynamics of substances with simultaneously negative values of ϵ and μ," Sov. Phys. Usp. **10**(4), 509–514 (1968).
2. J. Pendry, "Negative refraction makes a perfect lens," Phys. Rev. Lett. **85**(18), 3966–3969 (2000).
3. A. Poddubny, I. Iorsh, P. Belov, *et al.*, "Hyperbolic metamaterials," Nat. Photonics **7**(12), 948–957 (2013).
4. P. Shekhar, J. Atkinson, and Z. Jacob, "Hyperbolic metamaterials: Fundamentals and applications," Nano Convergence **1**(1), 14 (2014).
5. L. Ferrari, C. Wu, D. Lepage, *et al.*, "Hyperbolic metamaterials and their applications," Prog. Quantum Electron. **40**, 1–40 (2015).
6. N. Garcia, E. V. Ponizovskaya, and J. Xiao, "Zero permittivity materials: Band gaps at the visible," Appl. Phys. Lett. **80**(7), 1120–1122 (2002).
7. R. Ziolkowski, "Propagation in and scattering from a matched metamaterial having a zero index of refraction," Phys. Rev. E **70**(4), 046608 (2004).
8. A. Alú, M. Silveirinha, A. Salandrino, *et al.*, "Epsilon-near-zero metamaterials and electromagnetic sources: Tailoring the radiation phase pattern," Phys. Rev. B **75**(15), 155410 (2007).
9. G. Subramania, A. Fischer, and T. Luk, "Optical properties of metal-dielectric based epsilon near zero metamaterials," Appl. Phys. Lett. **101**(24), 241107 (2012).
10. J. Gao, L. Sun, H. Deng, *et al.*, "Experimental realization of epsilon-near-zero metamaterial slabs with metal-dielectric multilayers," Appl. Phys. Lett. **103**(5), 051111 (2013).
11. S. Suresh, O. Reshef, M. Zahirul Alam, *et al.*, "Enhanced nonlinear optical responses of layered epsilon-near-zero metamaterials at visible frequencies," ACS Photonics **8**(1), 125–129 (2021).
12. N. Kinsey, C. DeVault, A. Boltasseva, *et al.*, "Near-zero index materials for photonics," Nat. Rev. Mater. **4**(12), 742–760 (2019).
13. L. Vertchenko, M. Nikitin, and A. Lavrinenko, "Near-zero-index platform in photonics: tutorial," J. Opt. Soc. Am. B **40**(6), 1467–1482 (2023).
14. Y. Xu and H. Chen, "Total reflection and transmission by epsilon-near-zero metamaterials with defects," Appl. Phys. Lett. **98**(11), 113501 (2011).
15. J. Luo, W. Lu, Z. Hang, *et al.*, "Arbitrary control of electromagnetic flux in inhomogeneous anisotropic media with near-zero index," Phys. Rev. Lett. **112**(7), 073903 (2014).
16. R. Mei, J. Qin, D. Yan, *et al.*, "Breakdown of effective-medium theory in dielectric composites containing epsilon-near-zero constituents," Phys. Rev. B **109**(4), 045104 (2024).
17. H. Li, Z. Zhou, Y. He, *et al.*, "Geometry-independent antenna based on epsilon-near-zero medium," Nat. Commun. **13**(1), 3568 (2022).
18. M. Liu, S. Xia, W. Wan, *et al.*, "Broadband mid-infrared non-reciprocal absorption using magnetized gradient epsilon-near-zero thin films," Nat. Mater. **22**(10), 1196–1202 (2023).
19. I. Liberal, A. M. Mahmoud, Y. Li, *et al.*, "Photonic doping of epsilon-near-zero media," Science **355**(6329), 1058–1062 (2017).
20. X. Huang, Y. Lai, Z. Hong Hang, *et al.*, "Dirac cones induced by accidental degeneracy in photonic crystals and zero-refractive-index materials," Nat. Mater. **10**(8), 582–586 (2011).
21. D. I. Vulis, O. Reshef, P. Camayd-Munoz, *et al.*, "Manipulating the flow of light using Dirac-cone zero-index metamaterials," Rep. Prog. Phys. **82**(1), 012001 (2019).
22. Y. Li, C. Chan, and E. Mazur, "Dirac-like cone-based electromagnetic zero-index metamaterials," Light: Sci. Appl. **10**(1), 203 (2021).
23. T. Taliercio and P. Biagioni, "Semiconductor infrared plasmonics," Nanophotonics **8**(6), 949–990 (2019).
24. B. Wood, J. Pendry, and D. Tsai, "Directed subwavelength imaging using a layered metal-dielectric system," Phys. Rev. B **74**(11), 115116 (2006).

Optics EXPRESS

25. P. Yeh, *Optical waves in layered media*, vol. 61 (Wiley-Interscience, 2005).
26. L. Sun and K. W. Yu, "Strategy for designing broadband epsilon-near-zero metamaterials," J. Opt. Soc. Am. B **29**(5), 984 (2012).
27. S. M. Rytov, "Electromagnetic properties of a finely stratified medium," Soviet Physics JETP **2**, 466–475 (1956).
28. D. E. Fernandes and M. G. Silveirinha, "Enhancing the directional violation of kirchhoff's law of thermal radiation with a nonreciprocal wire medium," Phys. Rev. Appl. **20**(5), 054028 (2023).
29. A. Capretti, Y. Wang, N. Engheta, *et al.*, "Enhanced third-harmonic generation in si-compatible epsilon-near-zero indium tin oxide nanolayers," Opt. Lett. **40**(7), 1500–1503 (2015).
30. M. Z. Alam, I. D. Leon, and R. W. Boyd, "Large optical nonlinearity of indium tin oxide in its epsilon-near-zero region," Science **352**(6287), 795–797 (2016).
31. J. Nocedal and S. J. Wright, *Numerical optimization*, Springer Series in Operations Research and Financial Engineering (Springer, New York, 2006), 2nd ed.
32. P. Johnson and R. Christy, "Optical constants of the noble metals," Phys. Rev. B **6**(12), 4370–4379 (1972).
33. D. P. Nicholls, "A high–order spectral algorithm for the numerical simulation of layered media with uniaxial hyperbolic materials," J. Comput. Phys. **453**, 110961 (2022).

131.193.178.92 {ts '2025-01-10 14:07:44'}